Journal of Vacuum Science and Technology A

RESEARCH ARTICLE | SEPTEMBER 03 2024

Role of the magnetic layer interface, roughness, and thickness in the temperature-dependent magnetic properties of Al_2O_3/Co/CoO thin films deposited by magnetron sputtering

Aleksandr V. Kobyakov ; Gennadiy S. Patrin; Vasiliy I. Yushkov; Nikolay N. Kosyrev; Vasiliy A. Komarov; Yevgeny V. Tomashevich; Roman Yu. Rudenko

J. Vac. Sci. Technol. A 42, 053413 (2024)
https://doi.org/10.1116/6.0003772

JVST A
Journal of Vacuum Science & Technology A

ARTICLE

pubs.aip.org/avs/jva

Role of the magnetic layer interface, roughness, and thickness in the temperature-dependent magnetic properties of Al_2O_3/Co/CoO thin films deposited by magnetron sputtering

Cite as: J. Vac. Sci. Technol. A **42**, 053413 (2024); doi: 10.1116/6.0003772
Submitted: 22 May 2024 · Accepted: 12 August 2024 ·
Published Online: 3 September 2024

Aleksandr V. Kobyakov,[1,2,a)] Gennadiy S. Patrin,[1,2] Vasiliy I. Yushkov,[1,2] Nikolay N. Kosyrev,[3] Vasiliy A. Komarov,[1,2] Yevgeny V. Tomashevich,[4] and Roman Yu. Rudenko[1]

AFFILIATIONS

[1]Institute of Engineering Physics and Radioelectronics, Siberian Federal University, Krasnoyarsk 660041, Russia
[2]Kirensky Institute of Physics, Krasnoyarsk Scientific Center, Siberian Branch, Russian Academy of Sciences, Krasnoyarsk 660036, Russia
[3]Faculty of Agricultural Engineering, Achinsk Branch of Krasnoyarsk State Agrarian University, Achinsk 662155, Russia
[4]Institute of Chemistry and Chemical Technologies, Krasnoyarsk Scientific Center, Siberian Branch, Russian Academy of Sciences, Krasnoyarsk 660036, Russia

[a)]**Author to whom correspondence should be addressed:** nanonauka@mail.ru

ABSTRACT

Using the methods of atomic force and electron microscopy and the magneto-optical Kerr effect, the role of the interface, roughness, and thickness of the magnetic layer in the temperature-dependent magnetic properties of thin Al_2O_3–Co films with a naturally oxidized cobalt surface was studied. The layers were deposited by magnetron sputtering. The thickness of the cobalt layer varied from 2 to 100 nm. For the first time, the dependences of coercive forces and exchange displacements on the thickness of the cobalt film in the temperature range from 80 to 300 K were obtained and analyzed. The contribution to the coercive force and exchange displacement from the oxidized cobalt surface increases as the temperature decreases below 160 K. The magnitude of the contribution depends on the base material on which the cobalt film is deposited and is maximum for a cobalt film with a thickness of ~20 nm in the Al_2O_3/Co structure. A weakly magnetic layer was found at the Al_2O_3/Co interface. The behavior of the exchange bias in this layer is similar to the behavior of a ferromagnetic Co core with a naturally oxidized CoO shell. The thickness of this layer depends on the speed and order of deposition of the layers. When the order of deposition of layers (Co/Al_2O_3) changes, the behavior of the exchange displacement of the interface becomes similar to that observed in the ferromagnet/antiferromagnet system. That is, when the deposition order changes, the value of the exchange shift changes sign when the cobalt layer thickness is below 10 nm.

I. INTRODUCTION

The study of thin films with alternating magnetic and nonmagnetic layers is being emphasized by new fundamental research studies and practical applications.[1,2] One of the fields of research in this area is the exchange bias (EB) effect.[3] This effect is the basis of many applications in the field of spintronics, such as magnetic data storage, touch devices, and flexible electronics.

The exchange bias effect was discovered in the study of ferromagnetic (FM) Co particles coated with an antiferromagnetic (AFM) CoO shell.[4] Many studies are devoted to the study of EB effect phenomenology.[4–6] The main characteristics defining the properties of the EB effect are the shift magnitude, its sign, the asymmetry of the hysteresis loop, the blocking temperature (T_B is the temperature above which EB disappears), the training effect (a decrease in the hysteresis loop bias with a cyclic change in the

magnetic field), and the dependence of EB on time. Each of the characteristics is of independent interest for understanding the EB effect. The interaction at the FM-AFM interface results in the FM coercive force increasing with respect to the AFM single film, as well as the appearance of a hysteresis loop shift. The spin orientation at the AFM/FM interface can be very complicated, since in some cases, the crystallographic directions may not be equivalent in magnetic terms.

The AFM crystallinity, its morphology (e.g., surface roughness and grain size), and magnetic anisotropy are the most important parameters determining the value of EB.[7,8] Initially, it is suggested that only the AFM interface controls EB, i.e., EB is a purely interphase phenomenon where the role of the AFM bulk mass is limited to fixing interphase magnetic moments. However, the interface is always related to the AFM volume. Thus, the volume of AFM can affect the magnetic state of the interface, followed by an effect on EB. Now, there is much convincing evidence that the bulk magnetic state of AFM can affect EB.[9]

The FM layer crystallinity and its morphology are also the parameters that affect the value of EB. Thus, in flexible thin Co/CoO films grown by magnetron sputtering, there is an increase in the EB effect due to a decrease in the size of ferromagnetic particles and an increase in the FM/AFM contact area. In addition, the dependence of coercive force on film deformation has been demonstrated.[10] The studied Co/CoO thin film showed no worsening in all quality parameters after 500 bending cycles, which indicates its mechanical strength.

The interest of scientists in the Co/CoO system is increasing.[11–14] Cobalt (Co) is one of the 3d metals, and its distinctive features are high saturation magnetization, high Curie temperature, and a fairly high degree of conduction electron polarization.[15–17] It is known that the cobalt deposition conditions affect its phase composition, which is most often a mixture of phases.[18,19] In addition, cobalt is capable of oxidizing under atmospheric conditions. Thus, samples with an initial thickness of 5 nm or more are oxidized almost instantly. As a result, the top layer of the metal with a thickness of 2.5 nm turns into an oxide. With a greater cobalt thickness, but less than 5 nm, the oxidation time increases significantly and reaches a maximum value of 190 days. In this case, the cobalt layer with a thickness of less than 2.5 nm remains ferromagnetic for some time.[20]

Thus, problems related to the influence of structural, dimensional, and interface effects on the magnetic characteristics of thin-film structures come to the fore. Previously,[21] the relationship between the technological features of the Al_2O_3/Co film production and magnetic and structural properties at a cobalt thickness of ~100 nm has been investigated. Radu *et al.*[22] established the dependence of the EB effect on the thickness of wedge-shaped cobalt grown by HF spraying on an aluminum oxide substrate [*a*-phase Al_2O_3 (1120)] with a Co thickness of 2.7–40 nm. Next, the samples are exposed to air at room temperature. All samples have a positive EB below the blocking temperature and a negative EB near the blocking temperature. However, there is little information in the literature about the relationship between the cobalt film interface morphology and the EB effect, as well as the dependence of the EB effect on the thickness of cobalt on Al_2O_3 substrates at temperatures below room temperature.

This paper studies the EB effect in the Co/CoO system depending on the morphology of a sample with variable Co thickness at temperatures $T \leq 300$ K. Cobalt is deposited by the magnetron method on a glass substrate and on an Al_2O_3 layer on a glass substrate. The oxidation of cobalt occurs under the natural influence of atmospheric air at room temperature.

II. MATERIALS AND METHODS

The structures of glass/Co and glass/Al_2O_3/Co with a layer of aluminum oxide (Al_2O_3) and a magnetic layer of cobalt (Co) have been studied. The films are applied to a glass substrate (SiO_2) with an ultrahigh vacuum magnetron sputtering unit by "Omicron NanoTechnology" (Germany) with "Pfeiffer Vacuum" turbomolecular pumps. The substrate is placed in the elevator of the working chamber through the sample loading gateway system. Precipitation is carried out at a base pressure of 10^{-10} Torr in an argon atmosphere at a pressure of 3 mTorr (with a film thickness control system during the growth process). The substrate is cleaned by ion-plasma etching in a working chamber before the spraying process in an argon atmosphere. Spraying of all layers is carried out on a rotating substrate at its temperature $T \approx 373$ K.

The aluminum oxide layer is deposited by high-frequency magnetron sputtering of an Al_2O_3 target (99.99%). The cobalt layer is deposited by direct current magnetron sputtering from a Co target (99.95%). All targets are manufactured by "Scotech Limited," UK.

Two series of samples with variable thicknesses of cobalt (t_{Co}) layers from 2 to 100 nm are obtained for the study:

- Series 1: deposition of cobalt on a SiO_2 substrate (glass/Co/CoO).
- Series 2: deposition of cobalt on an Al_2O_3 layer (thickness 5 nm) deposited on SiO_2 (glass/Al_2O_3/Co/CoO).

The deposition rate of Al_2O_3 was 0.55 nm/min. The deposition rate of cobalt was $v_1 = 7.2$ nm/min. Additionally, samples with a cobalt deposition rate of $v_2 = 1.2$ nm/min were obtained to change the surface roughness of cobalt in samples with $t_{Co} = 10$ and 100 nm. After the films were deposited, the samples were kept in a high vacuum for 30 min. Next, the samples were taken out into the atmosphere, in which natural oxidation of the surface of the cobalt film occurred.

The surface morphology of all samples including the clean glass surface and the Al_2O_3 surface on the glass is studied by a Veeco MultiMode atomic force microscope (resolution 1 nm). The mean square roughness (Rms) and the diameter of the granules on the surface are investigated. The scanning transmission electron microscopy (STEM) image of the cross section of the structure is obtained by a Hitachi HT7700 transmission electron microscope. Transverse sections were prepared using a single-beam focused ion beam system (Hitachi FB2100). To protect it from destruction during the section preparation process, the sample was previously coated with a protective film of amorphous germanium (Ge). The average thicknesses are determined by means of the processing of the obtained images.

The chemical composition of the samples is studied by a SPECS electron spectrometer equipped with a PHOIBOS 150 MCD

9 hemispherical analyzer using a monochromatic Al K_α source (1486.6 eV). Electron gun characteristics were as follows: energy range 20 eV–5 keV and energy spread <1 eV. The pressure in the analytical chamber was 10^{-9} mbar. The spectra are obtained at room temperature. A coaxial surface charge neutralizer is used in the experiments. The experimental curve was decomposed into a series of peaks corresponding to the photoemission of electrons from atoms in different chemical environments. The spectra are processed by the CasaXPS program. The decomposition of the spectra into components with a combination of Gaussian and Lorentzian lines was carried out in accordance with the Shirley algorithm, after subtracting the nonlinear background caused by secondary electrons and photoelectrons losing energy. The binding energy measurement accuracy was ±0.1 eV. The decomposition of the $Co2p_{3/2}$ line is made with regard to the multiplet structure using the semiempirical approach described in the work of Biesinger *et al.*[23]

Magnetic measurements are carried out using the magneto-optical Kerr effect method (NanoMOKE-2) in the temperature range from 4.2 to 300 K. An external magnetic field was applied in the plane of the sample along the easy magnetization axis. Magnetization loops are obtained by the magneto-optical Kerr effect according to the method described in the work of Kosyrev *et al.*[24]

The operating principle of the NanoMOKE2 installation is based on recording the linear longitudinal Kerr effect ([the optical polarimetric scheme is classified as polarizer, sample, compensator, and analyzer (PSCA) and is as follows]. A laser diode (L) with a power of 2.5 mW generates radiation with a wavelength of 630–640 nm. Next, the beam becomes linearly polarized when passing through the polarizer P (the azimuthal angle is close to 90°). After that, the laser light is focused on the sample using an objective lens. Three lenses with different magnifications are provided; in this work, lenses that provide a diameter were used, probing beam 50 μm. The sample is mounted on a holder between the poles of a dipole electromagnet in such a way that the magnetic field strength vector H lies in the plane of incidence. Light, after reflection from the sample S, passes through a quarter-wave plate (C) (the azimuthal angle varies from 10° to 20°), the analyzer (A) (azimuth angle close to 0°), and a longitudinal Kerr effect detector (D). The detector performs an analysis of the polarization of laser radiation, namely, changes in the parameters of the polarization ellipse upon reflection for various values of the magnetic field and temperature (Fig. 1).

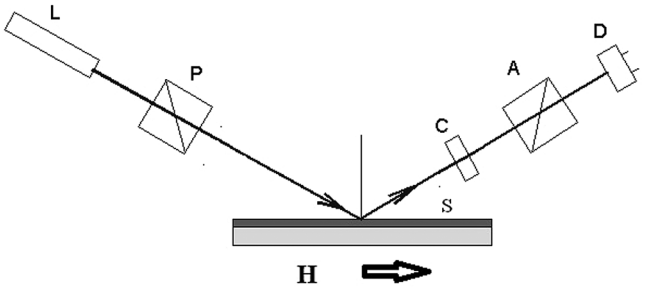

FIG. 1. Illustration of operation on the installation NanoMOKE2. L—laser diode, P—polarizer, C—quarter-wave plate, A—analyzer, D—detector S—sample, and H—magnetic field strength vector.

III. RESULTS

The results of STEM for both series of samples showed that the layers are fairly well separated [Figs. 2(a)–2(c)]. Figures 2(a) and 2(b) show the STEM images for glass/Al_2O_3/Co/CoO and glass/Co/CoO samples with cobalt deposition rates $v_1 = 7.2$ nm/min ($t_{Co} = 40$ nm). Figure 2(c) shows a STEM image of glass/Al_2O_3/Co/CoO, with cobalt deposition rates $v_2 = 1.2$ nm/min [Fig. 2(c)]. It should be noted here that as the speed increases, the interfaces become less clear and blurry.

A typical photoelectron spectrum characterizing the surface of a cobalt film is shown in Fig. 2(d). An example of a glass/Co/CoO sample with $t_{Co} = 20$ nm. The experimental curve is asymmetrical. After its development, a set of substances was obtained. A similar set of faces in the glass/Al_2O_3/Co/CoO samples are given as follows:

- Metallic Co with a main peak at 778.3 eV and two weak satellites (781.5 and 783.5 eV) at higher binding energies. The data correlate with the main cobalt peak and two plasmon loss peaks at 3.0 and 5.0 eV above the main peak making up the surface and volume plasmons, respectively, consistent with the work of Biesinger *et al.*[23]
- CoO oxide with a main peak at 780.3 eV and three satellites at higher binding energies (782.4, 785.8, and 786.8 eV). Although CoO and Co_3O_4 have similar positions for the main peak and the first satellite peak (~780 eV), the second strong satellite at about 786.8 eV is a distinctive feature of CoO and confirms the presence of oxide in the CoO spectrum.
- Weak peaks were presented, consistent with Co_3O_4 with a main peak at 779.4 eV and three satellites at higher binding energies (780.9, 783.7, and 788 eV).
- There is also a small contribution characteristic of carbon (the share is 8.6%).

The proportion of cobalt was 49.7% ($2p_{3/2}$), and the proportion of oxygen components was 41.6%. Note that the oxides CoO and Co_3O_4 are antiferromagnets with Néel temperatures TN ~ 290 and 40 K, respectively. Thus, multiple peaks in the spectrum confirm the formation of an oxidized layer on the surface of the cobalt film, which is an antiferromagnet.

Figures 3(a)–3(d) show the examples of SEM images and histograms of particle size distribution on the film surface for the samples: glass/Al_2O_3, glass/Co/CoO, glass/Al_2O_3/Co/CoO (v_1), and glass/Al_2O_3/Co/CoO (v_2), respectively. The cobalt thickness in the sample images is 10 nm. As expected, the surface has a granular structure. The grains have the correct shape in the nanometer range. In all the studied films, the grains are packed tightly. It has been determined from the particle size distribution histograms that the particle size in all samples varies from 10 to 32 nm.

Figure 4 shows the dependences of the average grain diameters (D—black line) and the average surface roughness of the samples (Rms—red line) on the cobalt layer thickness deposited on glass

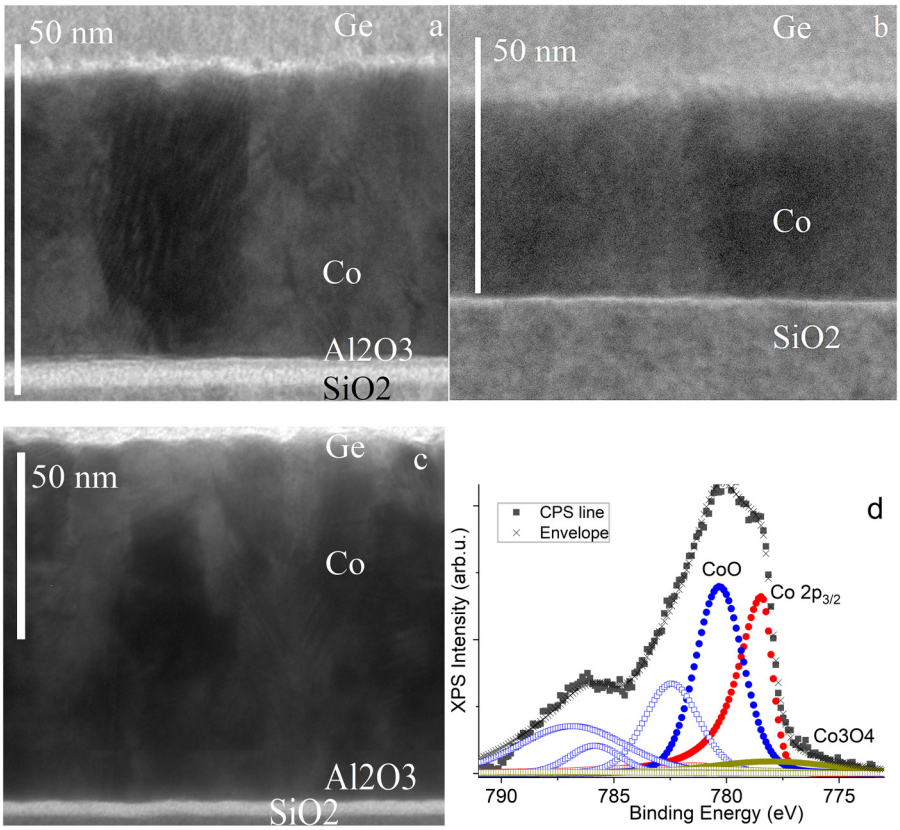

FIG. 2. STEM image of the sample glass/Al_2O_3/Co/CoO, cobalt deposition rates $v1 = 7.2$ nm/min (a), glass/Co/CoO, cobalt deposition rates v_1 (b), glass/Al_2O_3/Co/CoO, cobalt deposition rate $v_2 = 1.2$ nm/min (c), XPS spectra of the glass/Co/CoO film, with a cobalt thickness of 20 nm, obtained with Al K_α radiation excitement (1486, 6 eV). Co, CoO, and Co_3O_4. Solid circles are the main peaks, and open circles are the plasmons (d).

[Fig. 4(a)] and on aluminum oxide deposited on glass [Fig. 4(b)]. The corresponding patterns for both series of samples are similar to each other but differ in absolute values.

D(t) decreases while the cobalt layer thickness changes from 100 to 8 nm when it is deposited on SiO_2. For cobalt deposited on the Al_2O_3 layer, D(t) decreases while the cobalt thickness changes from 100 to 15 nm with a further decrease in the cobalt thickness, D(t) increases. For cobalt deposited on the Al_2O_3 layer, the dependence D(t) has another minimum at $t_{Co} \sim 4$ nm.

The roughness Rms(t) for both series of glass/Co/CoO and glass/Al_2O_3/Co/CoO samples behaves as follows. At cobalt thicknesses of 40–50 nm for both series of samples, a maximum roughness Rms(t) occurs. Furthermore, Rms(t) falls while cobalt thickness decreases and becomes minimal at $t_{Co} \sim 20$ nm for glass/Co/CoO samples and $t_{Co} \sim 8$ nm for glass/Al_2O_3/Co/CoO samples. With a further cobalt thickness decrease, a maximum Rms(t) occurs again at $t_{Co} \sim 8$ nm for glass/Co/CoO samples and $t_{Co} \sim 2$–3 nm for glass/Al_2O_3/Co/CoO samples.

It should be noted that the substrate after preliminary cleaning and cleaning by ion-plasma etching in the working chamber had an average roughness value of about 0.3 nm. The average grain size of the substrate is 22 nm. As expected, after the deposition of Al_2O_3 onto the substrate, the average roughness decreased to 0.26 nm, and the grain size on the Al_2O_3 surface decreased to 18 nm.[25]

When studying changes in coercive forces and exchange bias, magnetic hysteresis loops have been measured in the temperature range T = 4.2–300 K. The EB effect is characterized by an exchange bias field $H_E = (H_1 - H_2)/2$ and a coercive force $Hc = (|H_1| + |H_2|)/2$. H_1 and H_2 meet the values of the magnetic field, at which the magnetization of the hysteresis loop changes sign while magnetic field strength decreases and increases. At $t_{Co} \sim 2$ nm, weak hysteresis appears. Figure 4 shows the dependences of coercive forces on the cobalt film thickness for both series of samples at room temperature (Hc—blue line).

Figures 5(a) and 5(b) show the graphs of the coercive force dependence on the thickness of cobalt films for glass/Co/CoO and glass/Al_2O_3/Co/CoO samples, respectively. The graphs are presented for temperatures from 80 to 290 K. Coercive forces for all series of samples increase while the cobalt film thickness decreases from 100 to ~50 nm. At a thickness of ~50 nm, the Hc(t) dependence has a maximum. In glass/Al_2O_3/Co/CoO samples, at this cobalt film thickness, the maximum Hc disappears at temperatures below 180 K.

With a further decrease in the thickness of the cobalt layer to 10–15 nm, a feature arises. In both series of samples, a weakly pronounced maximum appears on the Hc(t) dependencies at temperatures below 170 K.

With a further decrease in the thickness of the cobalt layer to 6–10 nm, a minimum appears on the Hc(t) dependence, and with

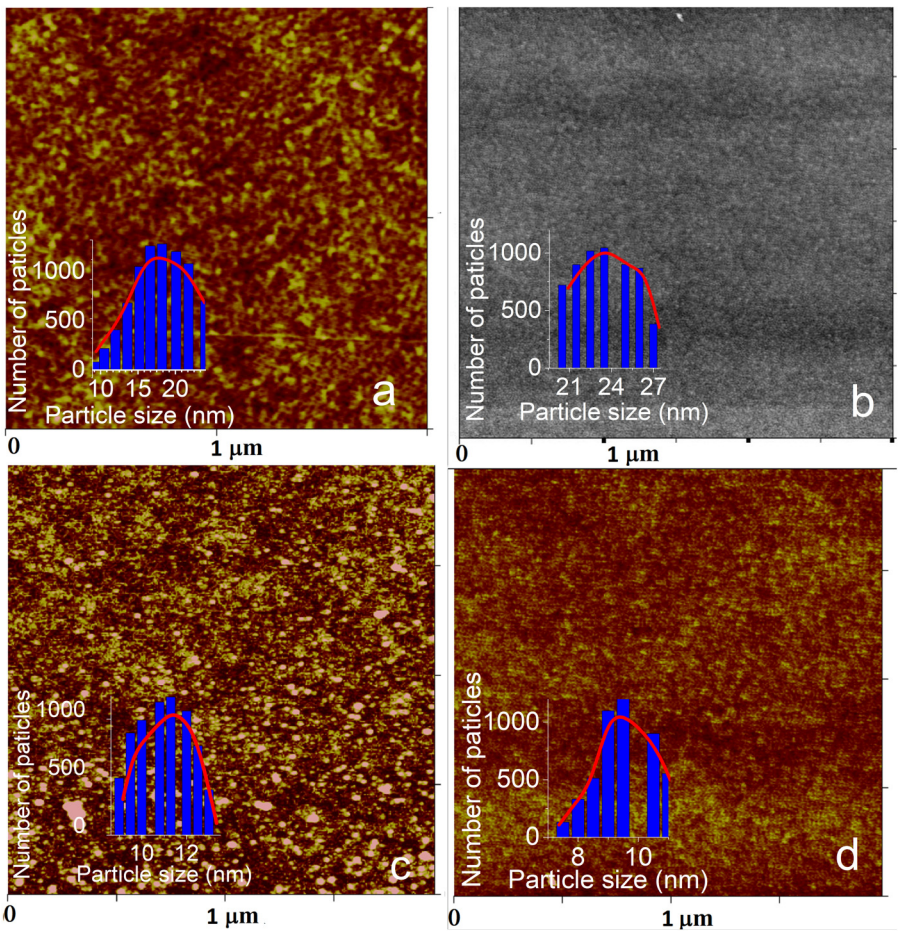

FIG. 3. SEM images and histograms of particle size distribution on the film surface for samples: glass/Al_2O_3 (a), glass/Co/CoO (b), glass/Al_2O_3/Co/CoO (v_1) (c), and glass/Al_2O_3/Co/CoO (v_2) (d). Cobalt thickness is 10 nm. Cobalt deposition rates are $v_1 = 7.2$ nm/min and $v_2 = 1.2$ nm/min.

a further decrease in the cobalt thickness to the minimum values, the coercive force increases sharply.

As expected, when there is a ferromagnetic cobalt and antiferromagnetic Co and Co_3O_4 particles in the film, an exchange bias effect occurs. We have presented the EB field as a dependence on the ferromagnetic layer thickness—$H_E(t)$. Figures 6(a) and 6(b) show the graphs of $H_E(t)$ dependencies for glass/Co/CoO and glass/Al_2O_3/Co/CoO samples, respectively. Graphs are presented for two series of samples for temperatures from 80 to 100 K up to 220–250 K, respectively.

When approaching room temperature, the $H_E(t)$ dependences become similar in both series of samples. However, when cooling below 190 K, there are differences. For glass/Co samples, a $H_E(t)$ maximum occurs at $t_{Co} \sim 13$–17 nm. At the same time, H_E has positive values. For glass/Al_2O_3/Co/CoO samples, a $H_E(t)$ maximum occurs at $t_{Co} \sim 20$ nm. At the same time, H_E becomes negative at temperatures below 170 K and at a t_{Co} of less than 10 nm. When the temperature decreases, the maximum height increases.

Figure 7(a) shows the temperature dependences of the exchange bias $H_E(T)$. For glass/Co/CoO samples, all $H_E(T)$ dependencies have a positive sign. For glass/Al_2O_3/Co/CoO samples, $H_E(T)$ dependences have a positive sign at temperatures above 200 K (discontinuous lines). However, when the temperature drops below ~190 K, the H_E value changes its sign and becomes negative for samples with $t_{Co} = 10$ nm or less. The temperature at which the H_E sign changes decreases as the cobalt thickness increases from 6 to 10 nm.

For a modified deposition sequence sample—glass/Co/Al_2O_3, on the contrary, there is a sharp increase in H_E below 200 K (green dots). For a glass/Co/Al_2O_3 sample with a reduced deposition rate (1.2 nm/min) at $t_{Co} = 10$ nm, the dependence is similar to the standard one, like for the FM/AFM (Co/CoO) system with a blocking temperature of $T_B \sim 166$ K (pink dots).

IV. DISCUSSION

The observed increase in the average grain size D(t) and the average surface roughness Rms(t) at thicknesses greater than 10 nm (see Fig. 4) is consistent with the results presented in other works.[26–29] The morphology of the cobalt film surface with thicknesses of more than 10 nm has been studied in the works.

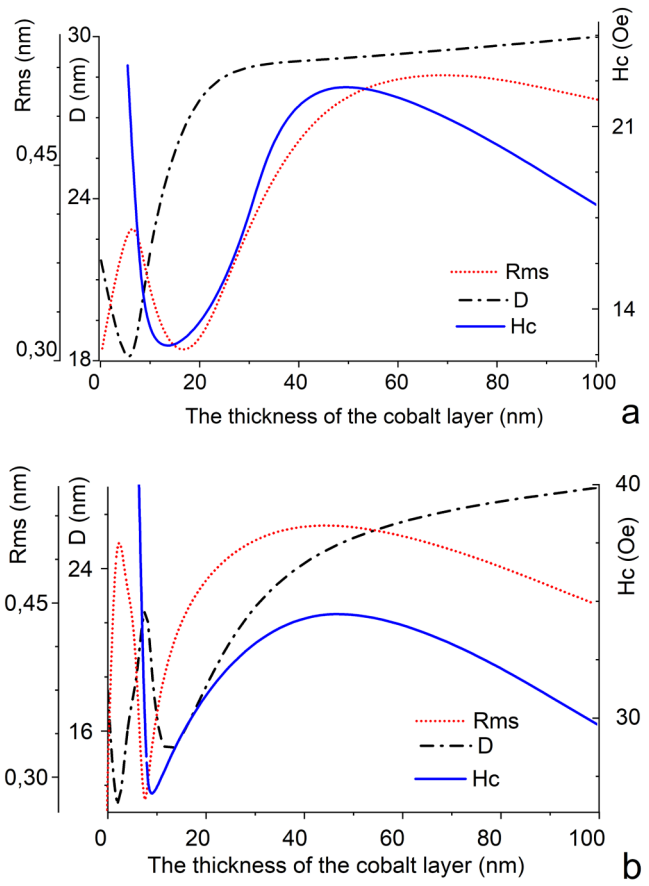

FIG. 4. Dependences of the average grain diameter (D), average roughness (Rms), and coercive force (Hc) on the thickness of the cobalt layer at a temperature of 300 K. (a) glass/Co/CoO and (b) glass/Al_2O_3/Co/CoO.

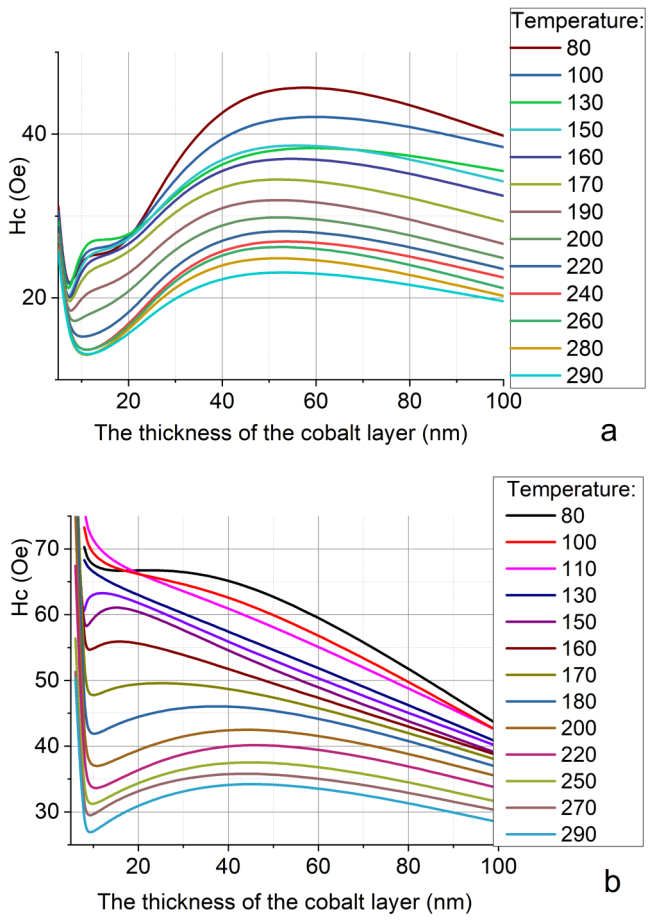

FIG. 5. Coercive force dependence on the thickness of cobalt at temperatures from 80 to 290 K. (a) glass/Co/CoO and (b) glass/Al_2O_3/Co/CoO.

The observed increase in the average grain size D(t) and the average surface roughness Rms(t) at thicknesses less than 10 nm is consistent with the results presented in other works.[30,31]

Such dependencies are related to the fact that in a cobalt film with a thickness of less than 10 nm, the energy of the Bloch-type domain boundary is greater than the Néel-type. Both the Néel and Bloch walls are in cobalt films at thicknesses of 20–30 nm. In cobalt films with a thickness of about 40–60 nm, the energies of the walls coincide. With even greater cobalt thicknesses, the energy of the Néel wall exceeds that of the Bloch wall. The energies of the Neel- and Bloch-type walls in films with a thickness of about 20–60 nm are comparable in magnitude.[32]

The change in the coercive force while the cobalt thickness increases is associated with a change in the size and energy of the Néel and Bloch walls and a change in roughness during the growth of the cobalt layer.

Since[33] the surface free energy of cobalt, which is 2.7 J m^{-2}, is significantly higher than that of SiO_2 and Al_2O_3 ≅ (0.95–1.9)J m^{-2}, it can be expected that the growth of cobalt proceeds by the Vollmer–Weber mechanism.[34,35] In this case, the film grows in the form of islands that merge together at higher thicknesses. This was shown with the growth of cobalt on MgO[36] and Si.[37]

Initially, the distance between the cobalt islands was quite large. The further deposition of cobalt results in an increase in the island's height and width. At this point, there is no electronic conductivity between the islands. There is no ferromagnetic interaction (there is a superparamagnetic ordering). The new islands result in an increase in roughness and a decrease in the average size of the granules (see Fig. 4). When a certain critical size of the islands is reached, a weak ferromagnetic interaction takes place between them.

With further cobalt deposition, there is a gradual transition from the island stage of growth to the formation of a continuous layer. At the same time, the roughness starts to decrease. It is minimal when the film is fully formed. At this point, the energy of the Bloch domain walls is slightly higher than that of the Néel

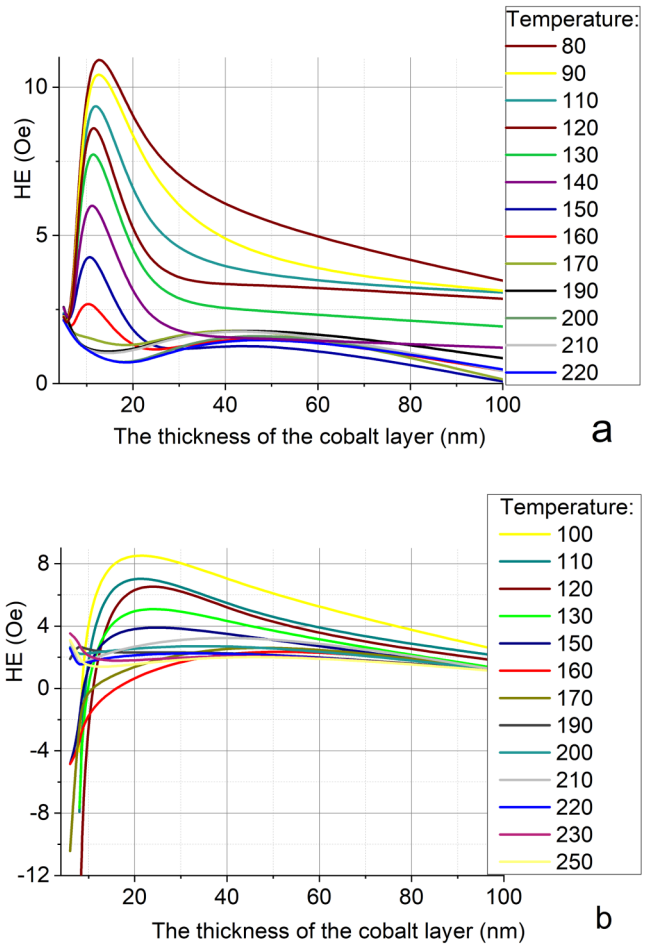

FIG. 6. Exchange bias dependence on the cobalt layer thickness at temperatures from 80 to 290 K. (a) glass/Co/CoO and (b) glass/Al_2O_3/Co/CoO.

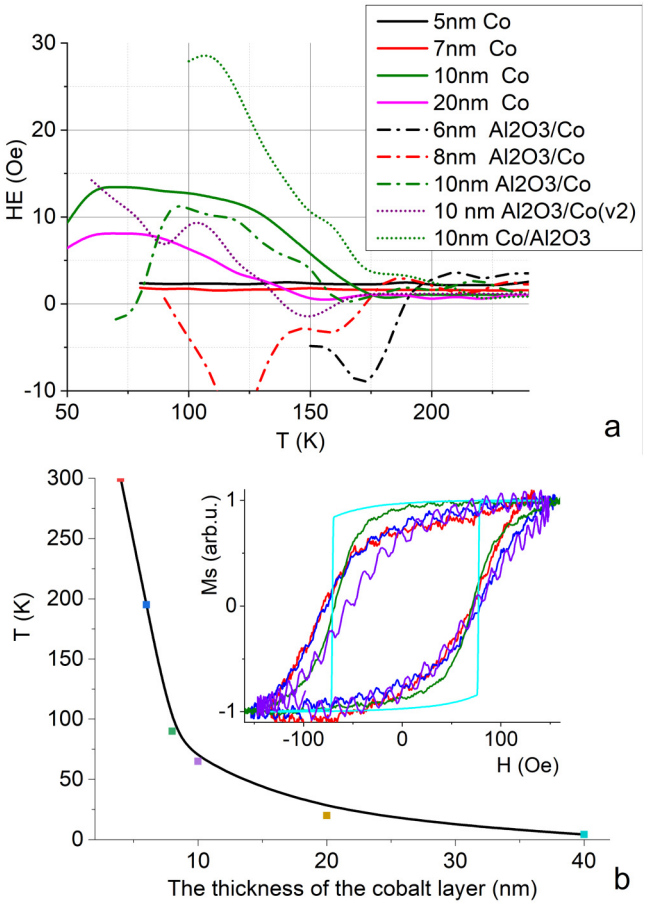

FIG. 7. Temperature dependences of the exchange bias H_E (a). Solid lines are glass/Co/CoO samples (v_1 = 7.2 nm/min). t_{Co} = 5, 7, 10, and 20 nm. Discontinuous lines are glass/Al_2O_3/Co/CoO samples: t_{Co} = 6, 8, and 10 nm. The dots are glass/Co/Al_2O_3, t_{Co} = 10 nm. and glass/Al_2O_3/Co/CoO (v_2 = 1.2 nm/min), t_{Co} = 10 nm. The temperature dependence at which the hysteresis loop becomes rectangular on the cobalt layer thickness in glass/Al_2O_3/Co/CoO (b) samples.

walls.[38] The size of the Néel walls decreases rapidly in this process, and the film thickness can be about 10–20 nm, depending on the material and the roughness of the surface on which cobalt is applied.

With a further increase in the cobalt thickness (more than 10–20 nm), the energy of the Néel-type walls increases. It results in an increase in roughness and in coercive force. The maximum coercive force at a cobalt thickness of 40–60 nm takes place on other substrates, for example, Si (at 50 nm) and GaAs (at 100 nm).[39] The energies and sizes of the Néel and Bloch domain walls become equal at the moment.

All the samples consisted of small grains. The average grain size in the samples ranges from 10 (for cobalt with a thickness of 2 nm) to 32 nm (for cobalt with a thickness of 100 nm), as shown in Fig. 4. There is a certain critical size below which the ferromagnetic order is violated. The critical size depends on the material itself, as well as on the impurities and their amount. For cobalt, this parameter can range from 10 to 30 nm.[40] When this size is exceeded, a strong exchange bond arises between the grains (some authors indicate that bonds are formed already at an average grain size of about 40 nm or less[41,42]).

A strong exchange bond between the grains results in a perpendicular magnetization component to the film plane in films with a cobalt thickness of more than 50 nm. At the same time, oxides are formed in the upper layer since the surface of small particles is chemically more active. Thus, the exchange interaction between grains plays a very significant role, smoothing and averaging the random distribution of the magnetocrystalline anisotropy of individual grains.[26] The structural configurations at the interface of the layers result in a dependence of H_E on the thickness of the ferromagnetic and antiferromagnetic layers.[1] For example, for CoO/Co bilayers, the EB field is inversely proportional to the

thickness of the ferromagnetic ($1/t_{FM}$), even for very small thicknesses (up to 2 nm) of the Co layer. This occurs when the layer is homogeneous.

The J_{FM}–A_{FM} bonding energy at the interface between FM and AFM determines the interaction. Provided that J_{FM}–$A_{FM} = K_{AFM} \times t_{AFM}$, the dependence of H_E on the thickness of the FM layer becomes decisive. K_{AFM} is the AFM magnetic anisotropy constant, and t_{AFM} is the AFM thickness. In this case, a dependence arises: $H_E = J_{FM-AFM}/M_{FM}t_{FM}$ (where M_{FM} is the FM magnetization). An increase in H_E with a decrease in the thickness of the FM layer is associated with an increase in disorder, both at the interface and on the cobalt surface.[1,42] The disorder increases with a decrease in the thickness of less than 20 nm. It results from a decrease in the diameter of the cobalt surface granules and the transition to a superparamagnetic state in both series of samples on the surface and at the Al_2O_3/Co interface (Figs. 4 and 6).

There is an increase in H_E when the temperature drops below 300 K. Figure 7(a) is related to the competition between J_{FM-AFM} and thermal energy. At low temperature, the magnetization stabilizes at the FM-AFM interface and H_E increases. T_B depends on the mess at the interface and on the AFM layer thickness. For thicker AFM layers, $T_B \approx T_N$, whereas in polycrystalline structures, $T_B < T_N$.[43–46] The dependence is in Fig. 6(a). The blocking temperature decreases while the cobalt thickness increases from 6 to 10 nm in glass/Al_2O_3/Co/CoO samples (Fig. 7—discontinuous lines). That is, structural inhomogeneities on the cobalt surface and at the Al_2O_3/Co interface result in a T_B change.

The H_E dependence in glass/Co/Al_2O_3 samples with cobalt thicknesses less than 10 nm at low temperatures has a negative H_E sign. It changes while the temperature increases. This behavior is similar to that of H_E for a structure with a ferromagnetic Co core and a naturally oxidized CoO shell.[1,47] However, in samples with lower roughness, the behavior of H_E is standard, like in the FM/AFM system [Fig. 7(a), glass/Al_2O_3/Co/CoO (v_2) sample deposited at a speed of $v_2 = 1.2$ nm/min, $t = 10$ nm]. The same type of H_E(T) dependence occurs when the deposition order of layers is changed (glass/Co/Al_2O_3 sample, $t_{Co} = 10$ nm).

It is known that the exchange bias field depends nonmonotonically on the thickness of the CoO shell and the greatest value of H_E is achieved when the Co core and the CoO shell have comparable dimensions.[48,49] Therefore, this occurs when the cobalt layer thickness is less than 10 nm. With a further increase in the thickness of the cobalt layer deposited on Al_2O_3, the dependence of H_E(T) also approaches the standard behavior of H_E like in the FM/AFM: Co/CoO system.

The Al_2O_3/Co interface is considered an Al_2O_3 matrix with cobalt grains embedded in it. This is indicated by an increased amount of roughness in small cobalt layer thicknesses (less than 10 nm) in glass/Al_2O_3/Co/CoO samples, compared with glass/Co/CoO samples. Magnetically, such a system has a superparamagnetic state. The violation of the ferromagnetic ordering is confirmed by a deviation from the squareness of the hysteresis loop when temperature decreases in glass/Al_2O_3/Co/CoO samples at $t_{Co} \leq 10$ nm. The dependence of the temperature at which the hysteresis loop becomes rectangular on the thickness of the cobalt layer is shown in Fig. 7(b). Below the temperatures indicated on the curve, the squareness of the hysteresis loop is disrupted. This confirms the magnetic disorder at the Al_2O_3/Co interface. The interface with

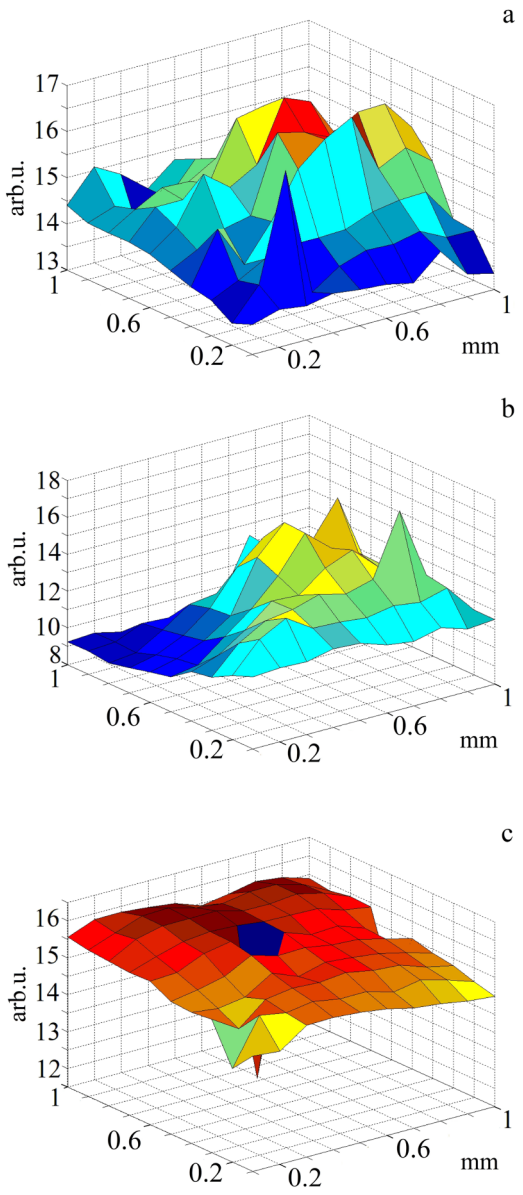

FIG. 8. Spatial saturation magnetization map for the glass/Al_2O_3/Co/CoO samples. T = 4 (a), 120 (b), and 300 K (c). Area is 1 mm^2.

the reverse sequence of Co/Al_2O_3 layers does not have a similar structure, and the hysteresis loop is rectangular in the entire temperature range (from 4 to 300 K). Thus, cobalt is deposited on the SiO_2 surface more evenly than on Al_2O_3. It takes place because the size of the granules on the surface decreases when Al_2O_3 is deposited on SiO_2, but the roughness increases in comparison with SiO_2.

To simulate the behavior of the saturation magnetization of the surface layer of a cobalt film, depending on temperature, we have constructed three-dimensional maps of saturation

magnetization. According to the temperature dependences of the exchange bias (Fig. 7), three temperatures have been selected for mapping. They are T = 4 K [Fig. 8(a)], T = 120 K [Fig. 8(b)], and T = 300 K [Fig. 8(c)]. The maps are constructed using data from magnetization loops obtained from one and the same place with an area of 1 mm^2 for each temperature (~400 loops). The maps are constructed for a glass/Al_2O_3/Co/CoO sample with a cobalt thickness of 100 nm.

According to spatial maps, it can be concluded that at T = 120 K, the saturation magnetization amplitude in the selected area is maximum (about 4 arb.u.), in contrast to the amplitudes at T = 4 and 300 K (about 2 arb.u.). This suggests that the magnetic surface roughness increases by about two times at temperatures near 120 K. The data indicate an increase in structural inhomogeneities near the temperature.

V. CONCLUSION

The structure, surface, and magnetic properties of glass/Co/CoO, glass/Al_2O_3/Co/CoO, and glass/Co/Al_2O_3 films have been systematically studied by means of atomic force, electron microscopy, and the method of the magneto-optical Kerr effect. The technological conditions of the deposition of samples and their structural and magnetic properties have been compared. For the first time, the dependences of coercive forces and exchange displacements on the thickness of the cobalt film in the temperature range from 80 to 300 K were obtained and analyzed. There are some main results of the work.

The dependences of the average grain diameters and average surface roughness of the samples depending on the thickness of the cobalt layer deposited on glass and aluminum oxide have been analyzed. An increase in roughness has been revealed at a cobalt thickness of about 8 nm and in the range of 40–60 nm at room temperature. The first increase is associated with the formation of the cobalt film structure, and the second with the equality of the energy of the Bloch and Néel walls in the film.

In the temperature dependences of coercive forces and exchange bias on the thickness of the magnetic layer, maxima appear at thicknesses of about 10 and 20 nm at temperatures from 80 to 190 K for glass/Co/CoO and glass/Co/Al_2O_3 films, respectively. The appearance of the exchange bias is associated with the formation of antiferromagnetic oxide CoO on the cobalt surface during sample preparation and the appearance of magnetic disorder at the Al_2O_3/Co interface.

The Al_2O_3/Co and Co/Al_2O_3 interfaces cannot be considered equivalent. When cobalt is deposited on Al_2O_3, an interface structure similar to a ferromagnetic Co core with a naturally oxidized CoO shell arises. The exchange bias of the structure changes sign at temperatures close to the blocking temperature of 166 K. The value of the blocking temperature depends on the structural disorder at the interface. Reducing the rate of cobalt deposition and changing the order of Co/Al_2O_3 deposition lower the structural disorder of the interface.

The results of experiments on growing thin films under various conditions (deposition rates, rotation, substrate materials, and temperatures) can provide additional information on the formation of interfaces during the growth of a thin cobalt film. The results may be of interest in the production of multilayer structures designed for information storage, touch sensors, and other devices.

ACKNOWLEDGMENT

The research was conducted according to the state assignment of the Ministry of Science and Higher Education of the Russian Federation and the Federal State Autonomous Educational Institution of Higher Education Siberian Federal University (No. FSRZ-2023-0008).

AUTHOR DECLARATIONS

Conflict of Interest

The authors have no conflicts to disclose.

Author Contributions

Aleksandr V. Kobyakov: Data curation (equal); Formal analysis (equal); Investigation (equal); Writing – original draft (equal); Writing – review & editing (equal). **Gennadiy S. Patrin:** Formal analysis (equal); Writing – review & editing (equal). **Vasiliy I. Yushkov:** Investigation (equal); Methodology (equal). **Nikolay N. Kosyrev:** Data curation (equal); Formal analysis (equal); Investigation (equal). **Vasiliy A. Komarov:** Data curation (equal); Investigation (equal); Validation (equal). **Yevgeny V. Tomashevich:** Data curation (equal); Investigation (equal). **Roman Yu. Rudenko:** Data curation (equal); Investigation (equal).

DATA AVAILABILITY

The data that support the findings of this study are available from the corresponding author upon reasonable request.

REFERENCES

[1]J. Nogués, J. Sort, V. Langlais, V. Skumryev, S. Surinach, J. S. Munoz, and M. D. Baró, Phys. Rep. **422**, 65 (2005).
[2]S. Sing, P. Kumar, A. Gupta, and D. Kumar, J. Magn. Magn. Mater. **513**, 167186 (2020).
[3]J. Nogués and I. K. Schuller, J. Magn. Magn. Mater. **192**, 203 (1999).
[4]W. H. Meiklejohn and C. P. Bean, Phys. Rev. **102**, 1413 (1956).
[5]M. Kiwi, J. Magn. Magn. Mater. **234**, 584 (2001).
[6]H. Ohldag, A. Scholl, F. Nolting, E. Arenholz, S. Maat, A. T. Young *et al.*, Phys. Rev. Lett. **91**, 017203 (2003).
[7]W. H. Meiklejohn, J. Appl. Phys. **33**, 1328 (1962).
[8]I. K. Schuller, R. Morales, and X. Batlle, J. Magn. Magn. Mater. **416**, 2 (2016).
[9]J. Sort, B. Dieny, and J. Nogués, Phys. Rev. **72**, 104412 (2005).
[10]Y. Sun, W. Tang, S. Chen, L. Liu, H. Liu, Jun-Yi Ge *et al.*, Adv. Phys. Res. **2**, 2200066 (2023).
[11]Suraj More, Bhavana Joshi, Ashwin Khadka, Edmund Samuel, Yongil Kim, Ali Aldalbahi *et al.*, Appl. Surf. Sci. **615**, 156386 (2023). .
[12]V. M. Marx, C. Kirchlechner, B. Breitbach *et al.*, Acta Mater. **121**, 227 (2016).
[13]Tianpei Zhou, Wanfei Xu, Nan Zhang, Zhiyi Du, Chengan Zhong, Wensheng Yan *et al.*, Adv. Mater. **31**, 1807468 (2019). .
[14]M. Mizoshiri, K. Yoshidomi, N. Darkhanbaatar, E. M. Khairullina, and I. I. Tumkin, Nanomaterials **11**, 3356 (2021).
[15]A. F. Franco, New J. Phys. **22**, 013017 (2020).
[16]H. Kahnouji, P. Kratzer, and J. Hashemifar, Phys. Rev. **99**, 035418 (2019).
[17]S. Andrieu, T. Haue, M. Gottwald, and Y. Garreau, Phys. Rev. Mater. **2**, 064410 (2018).

[18]Z. Zhang, X. Chen, X. Zhang, and C. Shi, Solid State Commun. **139**, 403 (2006).
[19]G. Patel, F. Ganss, R. Salikhov, S. Stienen, L. Fallarino *et al.*, Phys. Rev. B. **108**, 184429 (2023). .
[20]L. Smardz, U. Köbler, and W. Zinn, Appl. Phys. **71**, 5199 (1992).
[21]A. V. Kobyakov, G. S. Patrin, V. I. Yushkov, Y. G. Shiyan, R. Y. Rudenko, N. N. Kosyrev, and S. M. Zharkov, Magnetochemistry **8**, 130 (2022).
[22]F. Radu, M. Etzkorn, R. Siebrecht, T. Schmitte, K. Westerholt, and H. Zabel, Phys. Rev. **67**, 134409 (2003).
[23]M. C. Biesinger, B. P. Payne, A. P. Grosvenor, L. W. M. Lau, A. R. Gerson, and R. St. C. Smart, Appl. Surf. Sci. **257**, 2717 (2011).
[24]N. N. Kosyrev, V. Yu. Yakovchuk, G. S. Patrin, V. A. Komarov, E. N. Volchenko, and I. A. Tarasov, Tech. Phys. Lett. **47**, 107 (2021).
[25]J. Myers, James A. Throckmorton, and Rebecca A. Borrelli, Appl. Surf. Sci. **569**, 150878 (2021).
[26]W. Kozłowski, J. Balcerski, P. J. Kowalczyk, M. Cichomski, and W. Szmaja, Appl. Phys. A Mater. **123**, 169 (2017).
[27]A. Kharmouche, S.-M. Chérif, A. Bourzami, A. Layadi, and G. Schmerber, J. Appl. Phys. **37**, 2583 (2004).
[28]W. Gil, D. Görlitz, M. Horisberger, and J. Kötzler, Phys. Rev. **72**, 134401 (2005).
[29]M. F. Chioncel, H. S. Nagaraja, F. Rossignol, and P. W. Haycock, J. Magn. Magn. Mater. **313**, 135 (2007).
[30]Anup Kumar Bera, Pooja Gupta, Debi Garai, Ajay Gupta, and Dileep Kumar, Appl. Surf. Sci. Adv. **6**, 100124 (2021).
[31]Robert F. Renner and Knona C. Liddell, J. Mater. Res. **15**, 458 (2000).
[32]R. C. O'Handley, *Modern Magnetic Materials: Principles and Applications* (Wiley, New York, 1999).
[33]Henry P. Pinto, Risto M. Nieminen, and Simon D. Elliott, Phys. Rev. B **70**, 125402 (2004).
[34]O. Benamara, E. Snoeck, T. Blon, and M. Respaud, J. Cryst. Growth **312**, 1636 (2010).
[35]I. I. Pronin, D. A. Valdaitsev, A. S. Voronchikhin, M. V. Gomoyunova, S. F. Contri, S. Benedetti *et al.*, Tech. Phys. Lett. **31**, 494 (2005). .
[36]G. Sharma, U. P. Deshpande, D. Kumar, and A. Gupta, J. Appl. Phys. **112**, 023910 (2012).
[37]K. V. Sarathlal, D. Kumar, V. Ganesan, and A. Gupta, Appl. Surf. Sci. **258**, 4116 (2012).
[38]M. Ohring, *Materials Science of Thin Films Deposition and Structure* (Academic, New York, 2002).
[39]J. Islam, Y. Yamamoto, and H. Hori, J. Magn. Magn. Mater. **310**, 2234 (2007).
[40]E. C. Stoner and E. P. Wohlfarth, Philos. Trans. R. Soc. A **240**, 599 (1948).
[41]G. C. Hadjipanayis, J. Magn. Magn. Mater. **200**, 373 (1999).
[42]W. Szmaja, J. Grobelny, M. Cichomski, S. Hirosawa, and Y. Shigemoto, Acta Mater. **59**, 531 (2011).
[43]F. Radu and H. Zabel, Springer Tracts Mod. Phys. **227**, 97 (2008).
[44]T. Blachowicz and A. Ehrmann, Coatings. **11**, 122 (2021).
[45]R. L. Stamps, J. Phys. D: Appl. Phys. **33**, R247 (2000).
[46]S. K. Giri and T. K. Nath, J. Nanosci. Nanotechnol. **14**, 1209 (2014).
[47]S. Thomas, K. Reethu, T. Thanveer, M. T. Z. Myint, and S. H. Al-Harthi, J. Appl. Phys. **122**, 063902 (2017).
[48]J. B. Tracy and M. G. Bawendi, Phys. Rev. **74**, 184434 (2006).
[49]M. Feygenson, Y. Yiu, A. Kou, K.-S. Kim, and M. C. Aronson, Phys. Rev. **81**, 195445 (2010).